Construction and Calculation Analysis of Mechanical Model of Crushed Rock Pile Treatment of Foundation Earthquake

Yin Zhenyu

School of Civil and Transportation Engineering, Henan University of Urban Construction, Pingdingshan Henan 467041, China
E-mail: 30070101@hncj.edu.cn

Received 03 March 2023; Accepted 28 March 2023;
Publication 29 April 2023

Abstract

In recent years, earthquakes have occurred frequently at home and abroad, causing huge losses to the local society. Therefore, it is important to study the mechanical response of foundations under earthquakes. In this paper, firstly, gravel piles are selected as soft ground improvement materials, and A single bulk material pile section and a peripile soil section within the influence of a single pile are considered as a study unit, and the pore water discharge from the consolidation process is equal to the volume reduction of the unit, considering the consolidation deformation of the pile body, the composite foundation consolidation equation is derived, and the consolidation equation is solved by the separation variable method through the isostrain assumption and initial boundary conditions, and the average superporous water pressure of the soil between the body and the pile is obtained. Then, a more realistic non-uniform ground motion input method is adopted, and the seismic fluctuations are converted into equivalent loads on artificial boundary nodes through the Matlab program, and the equivalent loads are applied to the established viscoelastic artificial boundary by OpenSees software to realize ground motion input. Finally, a mechanical analysis model is established by

European Journal of Computational Mechanics, Vol. 31_5–6, 621–650.
doi: 10.13052/ejcm2642-2085.31564

hypothesis, and with the help of mode orthogonal theory and Hilbert yellow transform, the calculation method of ground seismic mechanical response based on non-uniform ground motion input is obtained. The results show that the effect of gravel pile encryption can reduce the accumulation rate and peak of super-static pore pressure during vibration, and the surface settlement of the site is reduced by 40–50% and the surface lateral shift is reduced by 30–50% after encryption; the drainage effect has a significant effect on reducing the accumulation rate of super-static pore pressure and the post-earthquake dissipation time of the soil during vibration, and the surface settlement is reduced by about 10–20% and the lateral shift is reduced by about 30–40% after increasing the drainage effect.

Keywords: Mechanical calculation, foundation mechanics, earthquake response, crushed stone pile, model construction.

1 Introduction

Since the 1960s, the composite establishment based on the model of rock heap fortifying delicate soil has been broadly utilized, completely appearing the noteworthy specialized and financial benefits of the composite establishment, provoking increasingly building innovation and logical analysts to get it and think about the composition, bearing component and stretch misshapen characteristics of the composite establishment.

The designing characteristics of the composite establishment shaped after the support of delicate soil or normal establishment will be significantly progressed [1]. It is basically based on the taking after two focuses: to begin with, the delicate soil is straightforwardly reinforced, which essentially increments the compactness of the soil, increments the shear quality, improves the compression resistance, and moves forward the energetic characteristics. The moment is the enhancement of bearing capacity and resistance to distortion of the composite establishment. The effect of the superstructure load on the composite foundation is borne by the reinforcement and the matrix in the composite foundation. Based on the pile-soil deformation coordination mechanism, most of the load will be borne by the reinforcement with higher stiffness and strength, so the load of the matrix will be greatly reduced, so the working efficiency of the composite foundation is improved and the engineering performance of the composite foundation is improved [2, 3].

Gravel pile has been widely used to treat soft foundation soil in engineering. People have carried out extensive and in-depth research on its

deformation and stress mechanism, and more and more research on consolidation. For example, in 1983, Charles J. A. and Watts K. S. carried out the indoor triaxial test of large-size bulk piles under rigid compression plates, and observed the stress-strain and consolidation characteristics of bulk piles. In 1992, Han Jie and Ye Shulin obtained a formula for calculating the degree of consolidation of gravel pile composite foundation considering well resistance and smearing under the condition of only radial seepage. Weidong Guo studied the plastic energy and generalized Brauns method to solve the composite foundation bearing capacity of flexible gravel piles with bulging damage, integral shear damage and corresponding damage forms. Tang X. W. studied the consolidation of a double-layer foundation under an ideal vertical drainage path. Wang Ruichun, Xie Kang, and others studied the consolidation of composite foundations with double-layer granular material piles under the stress concentration effect. Han J. and Ye S. L. proposed a simplified consolidation calculation method for gravel piles, etc [4]. Due to the large length-to-diameter ratio of piles in the composite foundation of crushed stone piles, the permeability of crushed stone piles is much greater than that of interpile soil, and the range of soil between piles under the influence of single piles is much smaller than the treatment depth of composite foundations, so most of the water pressure dissipation of soil superpores between piles is dissipated by horizontal penetration into the crushed stone pile body, and the vertical drainage effect is very small or even negligible.

2 Analytical Calculation of Consolidation of Composite Foundation with Bulk Material Piles Considering Consolidation Deformation

Barron has derived a theoretical solution for the consolidation of sand drain foundation under ideal conditions, Yoshikuni has given a free strain sand drain consolidation theory considering well resistance and smearing, and Xie Kanghe and Zeng Guoxi have studied the consolidation of sand drain foundation under equivalent strain conditions. On this premise, numerous researchers have done a part of the work on the expository arrangement of the union of the composite establishment of bulk fabric heaps, taking into consideration the characteristics of the composite establishment of bulk fabric heaps. For example, according to the basic characteristics of composite foundation, Xie Kanghe established an analytical theory of consolidation of composite foundation under simple conditions, taking into account the differences in stiffness and permeability between piles and coating areas

and foundation soil, and studied the radial and vertical combined seepage in the foundation [5, 6]. Han Jie and Zhang Aijun examined the impact of stretch concentration on the solidification of rock heap composite establishment. Wang Ruichun et al. examined the push concentration impact of the combination issue of composite establishments with double-layer bulk fabric heaps. Xu Yang et al. utilized a three-dimensional composite show to analyze the solidification issue of composite establishment with bulk heaps. Zhang Yuguo et al. considered the combination of composite establishments of granular fabric heaps with double-sided semi-permeable boundaries. Based on the guideline of breaking even with stream and disregarding the vertical waste of soil between heaps, Xing Haofeng et al. got a streamlined calculation equation for the combination of rock heap composite establishment.

Combined with specific examples, the method of this paper and related literature were used to The consolidation degree was calculated and compared with the literature. The results show that when the the results show that when the well diameter of the composite foundation of bulk material pile is relatively large, the two calculations are very similar. When the well diameter is small, the difference between the two is large. The method in this section is more suitable.

2.1 Establishment of the Calculation Model

When an infinite uniform load is applied to a composite foundation of bulk material piles, it can be considered that the force characteristics of each pile body and the soil around the pile are the same. Any force-deformed complex is selected as the analytical calculation model, as shown in Figure 1. H within the Figure is the overall thickness of the delicate soil layer; d_p is the diameter of the gravel pile; d_e is the outer diameter of soil between piles. According to experience, $d_e = 1.05\mathrm{L}$ (equilateral triangle arrangement), $d_e = 1.13\mathrm{L}$ (square arrangement), L is the pile center distance; δ_p, δ_s is the vertical deformation of pile and soil around pile under uniformly distributed load p_0; q_{hs} is the outspread pore water outpouring of the soil around the heap; q_{vp} is the vertical pore water outflow of the pile [7].

2.2 Derivation of Consolidation Equation

(1) The pile and soil around the composite foundation are homogeneous, the soil is saturated, and the solid particles and water are incompressible. (2) The seepage of water in composite foundation conforms to Darcy's law, and the permeability coefficient and compression coefficient are constant,

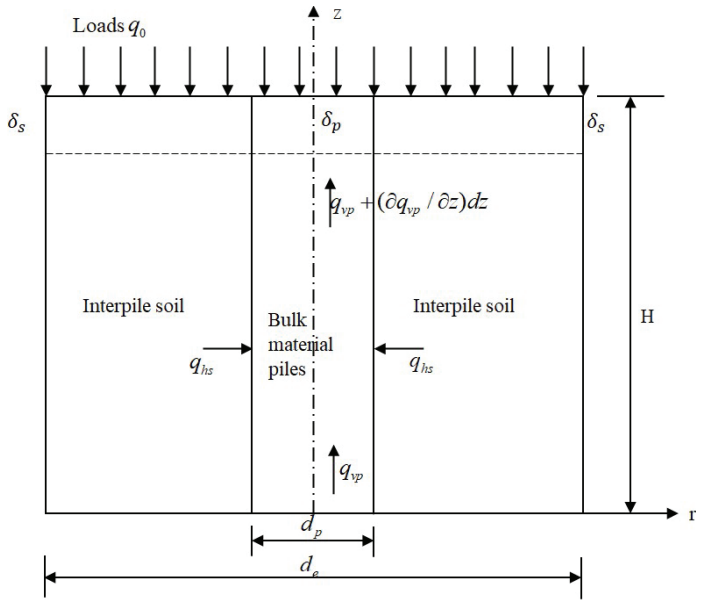

Figure 1 Typical computational model.

without considering the radial seepage of pile. (3) The consolidation deformation is small and the equal strain is established. (4) Only the vertical displacement of the complex is considered, and the vertical deformation between the pile and the soil around the pile is equal at the same depth. (5) The external load is applied once and remains unchanged, and meet the following requirements:

$$\bar{\sigma}_{\mathrm{p}} A_{\mathrm{p}} + \bar{\sigma}_{\mathrm{s}} A_{\mathrm{s}} = P_0 A \tag{1}$$

Within the same time increase dt, the relationship between the reasonable thrust increment of the unit body and the volume diminish of the unit body, and the compelling push increase is break even with to the abundance pore water stretch diminishment (effective stress rule), at that point there's

$$\frac{\partial u}{\partial t} = \frac{1}{m_{\mathrm{v}} v} \frac{\partial v_{\mathrm{s}}}{\partial t} \tag{2}$$

According to formula (2):

$$\frac{\partial v_{\mathrm{s}}}{\partial t} = \frac{\partial \bar{u}_{\mathrm{s}}}{\partial t} m_{\mathrm{vs}} A_{\mathrm{s}} \mathrm{d}z \tag{3}$$

According to Darcy's law:

$$\frac{\partial q_{\mathrm{vp}}}{\partial z}\mathrm{d}z = \partial \frac{k_{\mathrm{p}}}{\gamma_{\mathrm{w}}}\frac{\partial^2 \bar{u}_{\mathrm{p}}}{\partial z^2}A_{\mathrm{p}}\mathrm{d}z \tag{4}$$

Where, u_{p}, u_{s} is the average excess pore water pressure of the pile and the soil around the pile at t time; A_{p}, A_{s} is the sectional area of the pile and the soil around the pile; k_{p}, γ_{w} is the permeability coefficient of the pile and the weight of water; m_{v}, m_{vs} is the volume compression coefficient and the volume compression coefficient of the soil around the pile [8, 9].

Substitute Formula (2) and Formula (3) into Formula (1) to get:

$$\frac{\partial v_{\mathrm{s}}}{\partial t} = \frac{\partial \bar{u}_{\mathrm{s}}}{\partial t}m_{\mathrm{vs}}A_{\mathrm{s}}\mathrm{d}z\frac{\partial q_{\mathrm{vp}}}{\partial z}\mathrm{dz} = \partial \frac{k_{\mathrm{p}}}{\gamma_{\mathrm{w}}}\frac{\partial^2 \bar{u}_{\mathrm{p}}}{\partial z^2}A_{\mathrm{p}}\mathrm{d}z \tag{5}$$

Where, m_{vp} is the volume compression coefficient of gravel pile. Based on the presumption of rise to strain, it is gotten by substituting it into condition (1):

$$m_{\mathrm{vp}}\frac{\partial \bar{u}_{\mathrm{p}}}{\partial t} = m_{\mathrm{vs}}\frac{\partial \bar{u}_{\mathrm{s}}}{\partial t} \tag{6}$$

Substitute Formula (6) into Formula (5) to get:

$$\frac{\partial \bar{u}_{\mathrm{p}}}{\partial t}m_{\mathrm{vp}}A_{\mathrm{p}}\mathrm{d}z = \frac{k_{\mathrm{p}}}{\gamma_{\mathrm{w}}}\frac{\partial^2 \bar{u}_{\mathrm{p}}}{\partial z^2}A_{\mathrm{p}}\mathrm{d}z\partial\frac{\partial \bar{u}_{\mathrm{p}}}{\partial t}m_{\mathrm{vp}}A_{\mathrm{s}}\mathrm{d}z \tag{7}$$

Sorted out:

$$\frac{\partial u_x}{\partial t} = \beta_x \frac{\partial^2 u_x}{\partial z^2} \tag{8}$$

Which,

$$\begin{aligned} \beta_p &= \frac{k_p A_p}{m_{vp}\gamma_w(A_p + A_s)} = \alpha^2 C_{vp} \\ \beta_s &= \frac{k_s A_p}{\alpha^2 m_{vs}\gamma_w(A_p + A_s)} = \alpha^2 C_{vs} \end{aligned} \tag{9}$$

That's the differential condition of solidification of the rock heap composite establishment and the soil between heaps within the support zone. X represents the gravel pile and soil around the pile (including soil layer ① and layer ②).

According to the balance of force and isostrain assumption

$$\begin{aligned} \sigma_s A_s + \sigma_p A_p &= p_0 A_p \\ \sigma_s' m_{vs} &= \sigma_p' m_{vp} \end{aligned} \tag{10}$$

Where, σ_{x}, σ_x' is the total stress and effective stress respectively. When $\mathrm{t}=0$, $\sigma_x' = \sigma_{\mathrm{x}}$ combined with the two formulas in Formula (11), the excess pore water pressure of the pile and the soil around the pile is respectively:

$$u_{p0} = \frac{m_{vs}p_0}{m_{vs}\alpha^2 + m_{vp}(1-\alpha^2)}, \quad u_{s0} = \frac{m_{vp}p_0}{m_{vs}\alpha^2 + m_{vp}(1-\alpha^2)} \tag{11}$$

2.3 Boundary Conditions and Solution of Consolidation Equation

When the heap distance across proportion $\alpha = 1$, the soil around the heap is totally supplanted by rock heaps, and the solidification issue of the composite establishment is changed to the one-dimensional combination issue of the rock heaps [10]. From the figure, we can get the boundary conditions of consolidation under the impermeable condition of the upper drainage bottom (similar when both the upper and lower bottom surfaces are drained):

$$\begin{aligned} &\mathrm{t}=0, \quad 0 \le z \le H, \quad u_0 = u_{X0}; \\ &0 < t < \infty, \quad z = 0, \quad u = 0; \\ &t = \infty, \quad 0 \le z \le H, \quad u = 0 \end{aligned} \tag{12}$$

The continuous conditions of the upper layer and lower layer are:

$$\bar{u}_{\mathrm{s1}}|_{z=H_1} = \bar{u}_{\mathrm{s2}}|_{z=H_1}; \quad k_{\mathrm{s1}} \left.\frac{\partial \bar{u}_{\mathrm{s1}}}{\partial z}\right|_{z=H_1} = k_{\mathrm{s2}} \left.\frac{\partial \bar{u}_{\mathrm{s2}}}{\partial z}\right|_{z=H_1} \tag{13}$$

$$0 < t < \infty, \quad \left.\frac{\partial \bar{u}_{\mathrm{p}}}{\partial z}\right|_{z=H} = 0 \tag{14}$$

The pile is similar to the solution of Terzaghi's one-dimensional consolidation equation [11, 12]. The general solution of the pile consolidation equation is obtained from the boundary conditions and Fourier series by using the separation variable method:

$$\begin{aligned} \bar{u}_{\mathrm{p}} = \frac{2}{\pi} \sum_{m=1}^{\infty} \frac{1}{m} &\left[\bar{u}_{\mathrm{p}01} + \bar{u}_{\mathrm{p}02} + (\bar{u}_{\mathrm{p}01} - \bar{u}_{\mathrm{p}02}) \cos\left(\frac{m\pi H_1}{H}\right) \right] \\ &\times \sin\left(\frac{m\pi z}{H}\right) \mathrm{e}^{-m^2 \frac{\pi^2}{4} \beta_{\mathrm{vp}}} \end{aligned} \tag{15}$$

According to the separation variable method, the consolidation equation of the upper and lower layers of the soil around the pile is transformed into:

$$\frac{1}{\beta_{\mathrm{s1}}}\frac{1}{T}\frac{\partial T}{\partial t}=\frac{1}{X_{\mathrm{s1}}}\frac{\partial^2 X_{\mathrm{s1}}}{\partial x^2}=\frac{\beta_{\mathrm{s2}}}{\beta_{\mathrm{s1}}}\frac{1}{X_{\mathrm{s2}}}\frac{\partial^2 X_{\mathrm{s2}}}{\partial x^2}=-\lambda^2 \tag{16}$$

The answer is:

$$\begin{aligned} T &= Ae^{(-\lambda^2\beta_{s1}t)};\\ X_{s1} &= A_1\sin(\lambda z)+B_1\cos(\lambda z);\\ X_{s2} &= A_2\sin(a\lambda z)+B_2\cos(a\lambda z) \end{aligned} \tag{17}$$

3 Implementation of Inconsistent Ground Motion Input Method

When the source is near the building location, the seismic wave is shot into the structure at a certain point. Be that as it may, within the current seismic plan, in arrange to rearrange the recreation preparation, most of the seismic reaction examination of the structure is based on the suspicion that the seismic wave is a vertical occurrence [13]. This input method is reasonable for far-field earthquakes, while for near-field earthquakes, the spatial specificity of seismic waves is ignored, and the oblique incidence of seismic waves is the main factor causing such spatial differences. In order to better realize the reproduction effect of near-field earthquakes, the effect of the angular frequency of seismic waves must be considered in the seismic planning.

Based on the non-uniform seismic wave input method, this chapter converts the incident seismic wave into the equivalent load acting on the artificial viscoelastic boundary node through the Matlab language program and establishes the finite element model of the site soil through the open-source software OpenSees [14]. The comparable hub stack is connected to the location soil show to realize the reenactment prepare of the angled rate of seismic wave and examines the diffusing of the seismic wave beneath the conditions of diagonal: incident P wave and SV wave, The accuracy and effectiveness of the oblique incidence input method of seismic wave are verified, which lays the foundation for the seismic response of large reinforced concrete frame structures under the non-uniform incidence of seismic wave.

3.1 Near-field Wave Simulation

3.1.1 Viscoelastic artificial boundary

When using finite element method to analyze the incoherent input of seismic wave, the simulation of infinite field is the key. At present, the method to solve this problem usually adopts the method of intercepting the finite calculation area in the infinite field and applying the virtual artificial boundary on the finite area. After the artificial boundary is applied, the propagation characteristics of seismic waves at the artificial boundary should be the same as those in the original continuum in order to achieve accurate simulation of the original continuum. That is to say, the seismic waves are completely transmitted when they pass through the artificial boundary and no reflection effect occurs. Therefore, the accuracy of artificial boundary setting will directly affect the simulation effect of the original continuum.

At present, the artificial boundary is generally divided into global artificial boundaries and local artificial boundaries [17]. Since of its worldwide coupling, the worldwide fake boundary needs a parcel of time to calculate, whereas the neighborhood fake boundary is broadly utilized within the field of boundless field numerical reenactment since of its moderately little calculation time, simple execution, and tall calculation exactness. The commonly used local artificial boundary includes viscous boundary, viscoelastic boundary, transmission boundary, and composite boundary. As early as the last century, Lysmer J. et al. proposed that the establishment of viscous boundaries can be realized in finite element software. Since of its clear concept and simple usage, it has gotten to be one of the foremost broadly utilized boundary conditions in seismic reaction examination. Be that as it may, the thick boundary has self-evident low-frequency soundness issues, so it steadily created the transmission fake boundary Viscoelastic fake boundary. The viscoelastic fake boundary is created from the gooey counterfeit boundary, which overcomes the low-frequency soundness issue of the gooey boundary, and can be well combined with the expansive limited component computer program, and is broadly utilized within the approach wave investigation.

The viscoelastic artificial boundary is realized by setting a spring-damping physical system composed of discrete linear elastic dampers and viscous dampers in parallel on the intercepted boundary in the finite element software [18]. The system diagram is shown in Figure 2.

The solidness coefficient of the spring and the damping coefficient of the damper within the viscoelastic fake boundary are decided by the physical

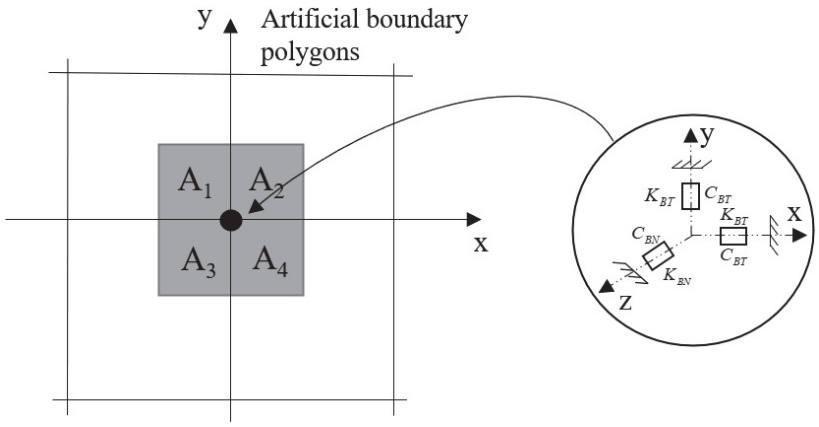

Figure 2 Viscoelastic artificial boundary equivalent physical system.

parameters of the location soil where the structure is found, respectively: A_1

$$\begin{aligned} K_{BT} &= \alpha_T \frac{G}{R} \\ C_{BT} &= \rho c_s \\ K_{BN} &= \alpha_N \frac{G}{R} \\ C_{BN} &= \rho c_P \end{aligned} \tag{18}$$

Where, K_{BN}, K_{BT} is the spring normal and tangential stiffness, C_{BN}, C_{BT} is the normal and tangential damping coefficient, R is the distance from the wave source to the artificial boundary point, c_{s}, c_{p} is the velocity of S wave and P wave respectively, G is the shear modulus of the medium, ρ Is the mass density of the medium, α_{T}, α_{N} is the tangential and normal viscoelastic artificial boundary parameters respectively. After a lot of numerical simulation, it is found that the artificial boundary parameters α_{T} is taken as 0.5–0.6 and α_{N} is taken as 1.00–1.33, satisfactory accuracy can be obtained [19].

In the process of seismic wave propagation, P wave and SV wave are two very important waveforms, which propagate in the form of body waves in the earth's internal medium. Both P and SV waves occur when incident from one medium into another. Conversion, P wave incident to the interface of different media, will produce reflected P wave and SV wave and refracted P wave and SV wave, SV wave incident to the interface of different media,

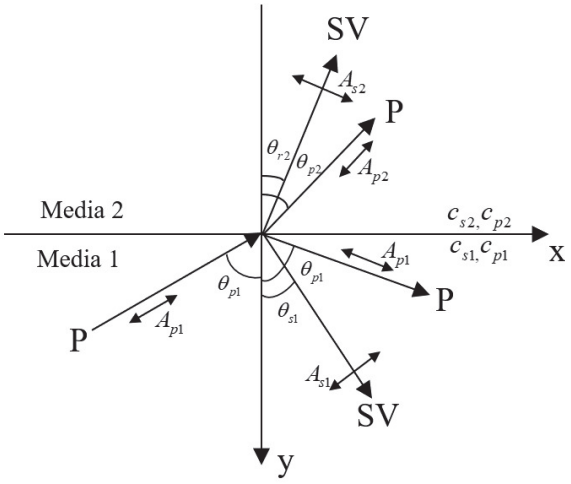

Figure 3 Refraction and reflection of P waves at the interface of the medium.

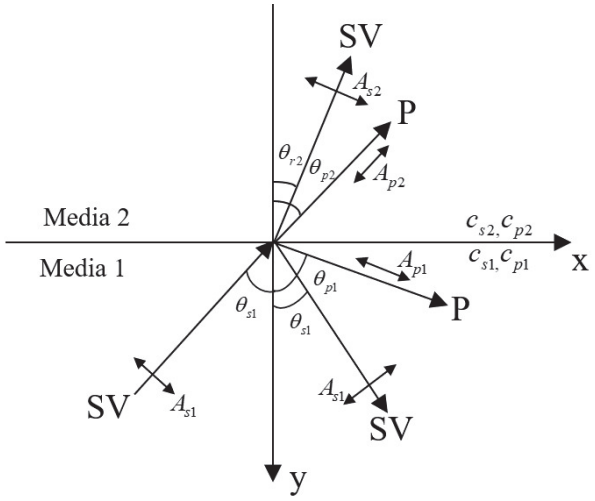

Figure 4 Refraction and reflection of SV waves at the interface of the medium.

will also produce reflected P wave and SV wave and refracted P wave and SV wave.

In the Figures 3 and 4, θ_{pi} and θ_{si} are the incident angles of P wave and SV wave respectively, A_{pi} and A_{si} are the corresponding amplitude of body wave.

In elastic media, the horizontal apparent wave velocities of P wave and SV wave at oblique incidence are:

$$\begin{aligned} c_{px} &= \frac{c_{p1}}{\sin\theta_{pi}} \\ c_{sx} &= \frac{c_{s1}}{\sin\theta_{si}} \end{aligned} \tag{19}$$

C_{px} and C_{sx} are the horizontal apparent wave velocities of P wave and SV wave respectively, and C_{p1} and C_{s1} are the wave velocities of P wave and SV wave in medium 1 respectively. According to Snell's law:

$$\frac{c_{s1}}{\sin\theta_{s1}} = \frac{c_{s2}}{\sin\theta_{s2}} = \frac{c_{p1}}{\sin\theta_{p1}} = \frac{c_{p2}}{\sin\theta_{p2}} = c_X \tag{20}$$

C_{s2} is the propagation speed of S wave in medium 2, and C_{p2} is the propagation speed of P wave in medium 2.

The free wave field generated by the oblique incidence of P wave and SV wave is:

$$u(x, y, t) = u\left(0, y, t - \frac{x}{c_x}\right) \tag{21}$$

The displacement expression of any point $(x_{\mathrm{i}}, y_{\mathrm{i}})$ in the two-dimensional model at any time p (p = 0,1,2…) is the relocation of the y-axis hub calculated by the one-dimensional time-domain limited component strategy, based on the traveling wave propagation characteristics, the displacement expression of the two-dimensional node $(x_{\mathrm{i}}, y_{\mathrm{i}})$ is:

$$u(x_i, y_i, p\Delta t) = u_0\left(y_i, p\Delta t - \frac{x_i}{c_x}\right) \tag{22}$$

If $p\Delta t - \frac{x_i}{c_x} \in (m\Delta t, (m+1)\Delta t)$, according to the linear interpolation method:

$$\begin{aligned} u(x_i, y_i, p\Delta t) = u_0(y_i, m\Delta t) &+ \frac{(p\Delta t - x_i/c_i) - m\Delta t}{\Delta t} \\ &\times [u_0(y_i, (m+1)\Delta t) - u_0(y_i, m\Delta t)] \end{aligned} \tag{23}$$

Concurring with the over prepare, the movement of hubs on the y-axis of the flat layered half-space limited component demonstrated at a diagonal frequency can be calculated by the one-dimensional time-domain limited component strategy [20]. At that point, concurring to the movement law of

the traveling wave, the vertical movement of a column of hubs illuminated can be expanded to the whole free wave field, and after that the movement of all hubs within the two-dimensional show can be extended to fathom the hub relocation time history of the two-dimensional free wave field [21, 22].

3.2 Implementation of Seismic Incidence

On the viscoelastic artificial boundary, the seismic wave input method is to convert the seismic wave effect into the equivalent load directly acting on the artificial boundary node, and convert the seismic wave effect into the stress condition imposed on the boundary point to realize the wave input. Figure 5 appears the realization strategy of wave input on viscoelastic counterfeit boundary hubs.

Where F_{BT} and F_{BN} represent the tangential and normal equivalent stress of artificial boundary node B respectively, $P_{BT} = F_{BT} \cdot \sum A_{\mathrm{i}}$ and $P_{BN} = F_{BN} \cdot \sum A_{\mathrm{i}}$. ZA represents the tangential and normal equivalent loads of artificial boundary node B respectively, $f_{BN}(x_B, y_B, t)$ and respectively represents the spring and damping on the artificial boundary node B. The normal stress and tangential stress produced by the device, $\sigma(x_B, y_B, t)$ and $\tau(x_B, y_B, t)$ are the normal of artificial boundary point B respectively. The stress of artificial boundary node B can be expressed as:

$$\begin{aligned} \sigma(x_{B,}y_{B,}t) &= F_{BN}(t) - f_{BN}(t) \\ \tau(x_{B,}y_{B,}t) &= F_{BT}(t) - f_{BT}(t) \end{aligned} \tag{24}$$

The normal stress $f_{BN}(x_B, y_B, t)$ and tangential stress $f_{BT}(x_B, y_B, t)$ generated by the spring and damper of artificial boundary node B are:

$$\begin{aligned} f_{BN}(x_B, y_B, t) &= C_{BN}u(x_B, y_B, t) + K_{BN}u(x_B, y_B, t) \\ f_{BT}(x_B, y_B, t) &= C_{BT}v(x_B, y_B, t) + K_{BT}v(x_B, y_B, t) \end{aligned} \tag{25}$$

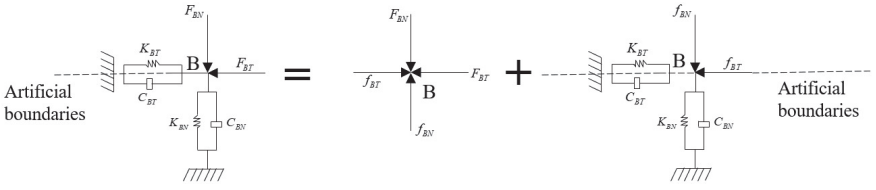

Figure 5 Schematic diagram of the wave input on the viscoelastic artificial boundary.

Substituting Equation (25) into (24), the equivalent stress of node B can be obtained as follows:

$$\begin{aligned} F_{BN}(x_B, y_B, t) &= \sigma(x_B, y_B, t) + C_{BN}u(x_B, y_B, t) + K_{BN}u(x_B, y_B, t) \\ F_{BT}(x_B, y_B, t) &= \tau(x_B, y_B, t) + C_{BT}u(x_B, y_B, t) + K_{BT}u(x_B, y_B, t) \end{aligned} \tag{26}$$

The equivalent load of artificial boundary node B can be obtained as follows:

$$\begin{aligned} P_{BN}(x_B, y_B, t) &= [\sigma(x_B, y_B, t) + C_{BN}u(x_B, y_B, t) \\ &\quad + K_{BN}u(x_B, y_B, t)] \sum A_i \\ P_{BT}(x_B, y_B, t) &= [\tau(x_B, y_B, t) + C_{BT}u(x_B, y_B, t) \\ &\quad + K_{BT}u(x_B, y_B, t)] \sum A_i \end{aligned} \tag{27}$$

Where C_{BN} is the tangential damper coefficient of artificial boundary node B, C_{BT} is the normal damper coefficient of artificial boundary node B, K_{BN} is the tangential spring stiffness of artificial boundary node B, K_{BT} is the normal spring stiffness of artificial boundary node B, and $C_{BN} = \rho c_p$, $C_{BT} = \rho c_s$, $K_{BN} = a_n \cdot (G/R)$, $K_{BT} = a_T \cdot (G/R)$.

On the off chance that the indistinguishable stack of fabricated boundary center B is required to achieve wave input, the thrust time history, speed time history, and movement time history of the free wave field must be gotten [23]. The motion timescale of the free wave field can be obtained by the unfolding action process technique of the free wave field presented in the previous section, the velocity timescale can be obtained by the central differential method, and the propulsion timescale can be obtained by the concentrated mass finite component strategy.

Agreeing with the speculation of lumped mass-constrained component procedure, the development of any center is because it was related to the component center particularly related to it [24, 25]. The proportionate stack connected to the boundary hub can be gotten from the movement to adjust the condition of the hub. The condition of movement of boundary hub B can be communicated as takes after:

$$m_B u_B + F_B + P_B = 0 \tag{28}$$

Where P_B is the concentrated external force vector, that is, the load excited by the boundary node, and $P_B = \{P_{Bx}, P_{By}\}$, u_B is the velocity time

history of the free wave field, F_B is the force determined by the stress-strain relationship:

$$F_B = K_0 u_{B0} \tag{29}$$

K_0 is the stiffness of the artificial boundary outer element to the boundary node B, and u_{B0} is the free wave field displacement time history of the node B and the adjacent boundary inner element.

Substitute Equation (29) into Equation (28) to obtain:

$$P_B = -(m_B u_B + K_0 u_{B0}) \tag{30}$$

The equivalent load P_B excited by the free wave field on the boundary node can be directly calculated according to (30), and the equivalent load on the artificial boundary can be obtained by substituting into Formulas (26) and (27) as follows:

$$\begin{aligned} P_{BN}(x_B, y_B, t) &= P_{By} + [C_{BN} u(x_B, y_B, t) + K_{BN} u(x_B, y_B, t)] \sum A_i \\ P_{BT}(x_B, y_B, t) &= P_{Bx} + [C_{BT} u(x_B, y_B, t) + K_{BT} u(x_B, y_B, t)] \sum A_i \end{aligned} \tag{31}$$

According to Equation (31), the equivalent load of the free wave field on the viscoelastic boundary node can be calculated. Realize the input of wave on the viscoelastic artificial boundary, its physical meaning is clear, and it is easy to compile Matlab program for solution and calculation [26].

Agreeing to the over hypothesis, an assistant calculation program is compiled with the assistance of Matlab dialect to change over the seismic wave into the comparable stack acting on the manufactured boundary hub. The limited component demonstrates of viscoelastic counterfeit boundary location soil is built up in OpenSees, and the comparable stack is connected to the counterfeit boundary hub to total the conflicting input of seismic waves.

4 Calculation of Seismic Response of the Layered Foundation

As a common building-bearing body, the reaction characteristics of layered establishments beneath seismic tremors have an awesome affect on the seismic security of buildings. At present, the study of seismically accelerated laminar response remains within the scope of field perception, demonstration tests and numerical studies. In recent years, some theoretical solutions have emerged. Luan Maotian et al. established a complete form of simplified

analytical solution for the vibration characteristics and seismic response of laminar sites; Fan Liuming et al. studied the time course algorithm for seismic effects of laminar soil sites and the interface wavelet algorithm for the dynamic response of laminar soil sites under the action of obliquely incident seismic waves. Xing Hailing et al. studied the equivalent linearization method for calculating the surface response spectrum of layered site by using the bedrock response spectrum; Wang Zairong et al. discussed the damping matrix modeling in the seismic response analysis of layered sites; Nimtaj et al. established a calculation method for nonlinear response of layered foundation; Zeng et al. studied the calculation method of dynamic response of multi-layer layered site under the action of plane shear wave; Liang et al. studied the dynamic stiffness matrix and Green's function of porous elastic layered foundation; Akiyoshi et al. studied the calculation method of site effect and nonlinear response of layered foundation. As a kind of extremely complex random signal, the frequency and amplitude characteristics of seismic wave change greatly with time. The time variation of seismic wave frequency and amplitude has a great impact on the seismic response of rock and soil [27].

On the basis of establishing a generalized analysis model, with the help of elastic wave theory and Hilbert Huang transform (HHT), taking the joint seismic time-frequency domain as the analysis scope, the time-frequency amplitude characteristics of seismic waves are considered, and the time-frequency calculation method of seismic response of laminated foundation is derived.

4.1 Formula Derivation

Select the soil column per unit range within the layered location for investigation, partition the soil column into a limited number of investigation components, utilize the wave hypothesis to infer the stretch state of each investigation component beneath the activity of seismic waves, and set up the stretch adjust the condition of the examination component. On this basis, combined with the boundary conditions and the Hilbert-Huang transform considering the time-frequency-amplitude characteristics of seismic waves, the time-frequency analysis method of seismic response of the layered site is obtained. The analysis in this paper is based on the following assumptions: (1) The geotechnical material in the site is homogeneous isotropic; (2) The overlying bedrock under the site is rigid, that is, the deformation of the overlying bedrock is not considered in the derivation

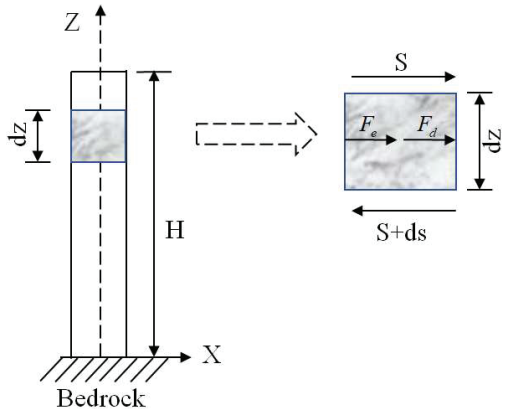

Figure 6 Analysis model.

process; (3) The influence of Rayleigh surface waves generated by waveform conversion on the field surface is not considered.

In Figure 6, the upper shear force of the analysis unit is S, the lower shear force is S + dS, F_e is the seismic force of the analysis unit, and F_d is the resistance force. The calculation formula of each force is as follows:

$$F_{\mathrm{c}} = \rho \mathrm{d}z \left[\frac{\partial^2 v}{\partial t^2} + \ddot{v}_{\mathrm{g}}(t) \right] \tag{32}$$

$$F_{\mathrm{d}} = c \mathrm{d}z \frac{\partial v}{\partial t} \tag{33}$$

$$S = G\gamma = G \frac{\partial v}{\partial \mathrm{t}} \tag{34}$$

Where: ρ is the density of rock and soil mass; v is shear displacement; γ is shear strain; G is shear modulus; c is the viscosity coefficient. Considering the force balance of the analysis unit, we can get:

$$F_e + F_d - \frac{\partial S}{\partial z} dz = 0 \tag{35}$$

Substitute Formulas (32)–(34) into 4 to obtain:

$$\frac{\partial^2 v}{\partial t^2} + \frac{c}{\rho} \frac{\partial v}{\partial t} - \frac{G}{\rho} \frac{\partial^2 v}{\partial z^2} = -\ddot{v}_g(t) \tag{36}$$

$v = \varphi(t)Y(t)$. $\varphi(t)$ is the mode function with dimension 1, and $Y(t)$ is the time function of the mode. According to the separation variable method,

and each item is multiplied by $\rho z\varphi$, Equation (5) can be converted into the following form:

$$\sum_{1}^{\infty}\varphi^2\rho z\frac{\partial^2 Y}{\partial t^2}+c\sum_{1}^{\infty}z\varphi^2\frac{\partial Y}{\partial t}-\frac{GY}{\rho}\sum_{1}^{\infty}\rho z\varphi\frac{\partial^2\varphi}{\partial z^2}=-\varphi z\rho\ddot{v}_g(t) \quad (37)$$

At this time, formula (37) contains only two variables, t, and z, which can be obtained according to the orthogonality of vibration mode:

$$\left(\sum_{0}^{H}\varphi^2\rho z\right)\frac{\partial^2 Y}{\partial t^2}+\left(\sum_{0}^{H}cz\varphi^2\right)\frac{\partial Y}{\partial t}-\frac{GY}{\rho}\left(\sum_{0}^{H}\rho z\varphi\frac{\partial^2\varphi}{\partial z^2}\right)$$
$$=-\left(\sum_{0}^{H}\varphi z\rho\right)\ddot{v}_g(t) \quad (38)$$

Where λ is the critical damping ratio, ω is the natural vibration frequency. Divide each item in Equation (38) by $\sum_0^H \rho z\varphi^2$ and $\frac{GY}{\rho}$, and separate Equation (38) into:

$$\frac{\partial^2 Y}{\partial t^2}+2\lambda\omega\frac{\partial Y}{\partial t}+RY\frac{G}{\rho}=-\left(\frac{\sum_0^H\varphi z}{\sum_0^H\varphi^2 z}\right)\ddot{v}_g(t) \quad (39)$$

$$\frac{\partial^2\varphi}{\partial z^2}+R\varphi=0 \quad (40)$$

Where: R is the undetermined constant. In this study, rock, and soil materials are mainly subject to shear deformation, and the stiffness K of the material is determined by G and geometric dimensions, so there is the following relationship, $\omega^2 = \mathrm{K}/\rho = \mathrm{RG}/\rho$, accordingly, formula (39) can be written as:

$$\frac{\partial^2 Y}{\partial t^2}+2\lambda\omega\frac{\partial Y}{\partial t}+\omega^2 Y=-\left(\frac{\sum_0^H\varphi z}{\sum_0^H\varphi^2 z}\right)\ddot{v}_g(t) \quad (41)$$

For Equation (40), $R=(\varsigma/z)^2$, Equation (40) is converted to:

$$\frac{\partial^2\varphi}{\partial\varsigma^2}+\varphi=0 \quad (42)$$

Equation (42) is a second-order homogeneous linear equation, which can be solved as $\varphi=\cos(\sqrt{R}z)+\sin(\sqrt{R}z)$, according to boundary conditions $\mathrm{Z}=\mathrm{H}$, $\partial\varphi/\partial z=0$,

$$R=\left(\frac{\pi}{4H}\right)^2 \quad (43)$$

The vibration mode function can be obtained by solving Equation (43):

$$\varphi = \cos\left(\frac{\pi z}{4H}\right) + \sin\left(\frac{\pi z}{4H}\right) \tag{44}$$

Substitute the vibration mode function (44) into Equation (41) to obtain:

$$\frac{\partial^2 Y}{\partial t^2} + 2\lambda\omega\frac{\partial Y}{\partial t} + \omega^2 Y = -\frac{16H^2(\sqrt{2}-1)}{\pi^2}\ddot{v}_g(t) \tag{45}$$

Equation (45) is a non-homogeneous second-order linear differential equation, and its general solution is calculated as follows:

$$Y = \frac{H^2\ddot{v}_{\mathrm{g}}^2}{\pi^2\omega^2(1-\lambda^2)^{0.5}}\mathrm{e}^{[\lambda+(1-\lambda^2)^{0.5}]_{\omega t}} \tag{46}$$

At this time, the shear displacement is:

$$v = \left[\cos\left(\frac{\pi z}{4H}\right) + sin\left(\frac{\pi z}{4H}\right)\right]\frac{H^2\ddot{v}_{\mathrm{g}}^2}{\pi^2\omega^2(1-\lambda^2)^{0.5}}\mathrm{e}^{[\lambda+(1-\lambda^2)^{0.5}]_{\omega t}} \tag{47}$$

On this basis, the displacement response and acceleration response of the layered site can be obtained by differentiating the shear displacement of the site once and twice respectively.

$$\frac{\partial v}{\partial t} = \omega[\lambda + (1-\lambda^2)^{0.5}]\left[\cos\left(\frac{\pi z}{4H}\right) + sin\left(\frac{\pi z}{4H}\right)\right] \times \frac{H^2\ddot{v}_{\mathrm{g}}^2}{\pi^2\omega^2(1-\lambda^2)^{0.5}}\mathrm{e}^{[\lambda+\left(1-\lambda^2\right)^{0.5}]_{\omega t}} \tag{48}$$

$$\frac{\partial^2 v}{\partial t^2} = \omega^2[\lambda + (1-\lambda^2)^{0.5}]^2\left[\cos\left(\frac{\pi z}{4H}\right) + sin\left(\frac{\pi z}{4H}\right)\right] \times \frac{H^2\ddot{v}_{\mathrm{g}}^2}{\pi^2\omega^2(1-\lambda^2)^{0.5}}\mathrm{e}^{[\lambda+(1-\lambda^2)^{0.5}]_{\omega t}} \tag{49}$$

4.2 Time-frequency Calculation Method of Composite Foundation

According to the comprehensive analysis formulas (47)–(49), the acceleration amplitude and frequency of seismic wave ω It has a great influence on the seismic response of the site. As a complex and unstable signal,

the acceleration amplitude $\ddot{v}_{\mathrm{g}}^2$ and frequency ω of seismic wave change with time. Therefore, the acceleration amplitude $\ddot{v}_{\mathrm{g}}^2$ and frequency ω in Equations (47)–(49) are the quantities that change with time, representing the acceleration amplitude and instantaneous frequency corresponding to time t. The premise of calculating the site seismic response by using Equations (47)–(49) is that the amplitude signal and frequency signal of complex seismic wave can be separated to obtain the instantaneous amplitude and frequency of seismic wave at each time [28].

The Hilbert-Huang transform (HHT) decomposes a complex, unstable seismic wave signal into a series of eigenmode functions by empirical mode decomposition and calculates the instantaneous frequency of each eigenmode function. So far, the random seismic signal has been decomposed into a three-dimensional signal including time, amplitude and frequency. The response of the laminar site under arbitrary seismic wave excitation is obtained by substituting each eigenmodal function into Equations (47)–(49) and accumulating the calculated results of each eigenmodal function. Therefore, Equations (47)–(49) can be further expressed as Equations (50)–(52), where n is the number of eigenmode functions.

$$v = \sum_{1}^{n} \left[\cos\left(\frac{\pi z}{4H}\right) + sin\left(\frac{\pi z}{4H}\right)\right] \frac{H^2 \ddot{v}_{\mathrm{g}}^2}{\pi^2 \omega^2 (1-\lambda^2)^{0.5}} \mathrm{e}^{[\lambda + (1-\lambda^2)^{0.5}]_{\omega t}} \tag{50}$$

$$\frac{\partial v}{\partial t} = \sum_{1}^{n} \omega[\lambda + (1-\lambda^2)^{0.5}] \left[\cos\left(\frac{\pi z}{4H}\right) + sin\left(\frac{\pi z}{4H}\right)\right] \times \frac{H^2 \ddot{v}_{\mathrm{g}}^2}{\pi^2 \omega^2 (1-\lambda^2)^{0.5}} \mathrm{e}^{[\lambda + (1-\lambda^2)^{0.5}]_{\omega t}} \tag{51}$$

$$\frac{\partial^2 v}{\partial t^2} = \sum_{1}^{n} \omega^2 \left[\lambda + (1-\lambda^2)^{0.5}\right] \left[\cos\left(\frac{\pi z}{4H}\right) + sin\left(\frac{\pi z}{4H}\right)\right] \times \frac{H^2 \ddot{v}_{\mathrm{g}}^2}{\pi^2 \omega^2 (1-\lambda^2)^{0.5}} \mathrm{e}^{[\lambda + (1-\lambda^2)^{0.5}]_{\omega t}} \tag{52}$$

The steps to calculate the site seismic response using the method established in this paper are as follows: (1) Empirical mode decomposition of input seismic wave is performed to obtain its eigenmode function; (2) According to the decomposition results, the proper order eigenmode function is selected

to calculate its instantaneous frequency; (3) The instantaneous acceleration amplitude and instantaneous frequency of each eigenmode function are brought into Formula (50)–(52) to calculate the seismic response of the site under the action of each eigenmode function; (4) The seismic response of the site under the action of each eigenmode function is accumulated to obtain the seismic response of the site under the action of input seismic wave [29].

4.3 Verification of High Gravity Model Test

4.3.1 Model test layout

This chapter uses 40 geocentrifuges and an airborne shaking table to treat the horizontal site as a special condition of the inclined site. Three sets of super gravity model tests on horizontal site were designed and carried out. The compaction effect of foundation treated by gravel pile and the influence law of drainage response to seismic responses such as acceleration, excess pore pressure and settlement were systematically compared and analyzed. Secondly, based on the existing analytical solutions, the semi-analytical expressions of horizontal and vertical seepage flow in the foundation treated by the lower crushed stone pile with vibration are derived. The model test results verify the correctness of the model test and analyze the horizontal and vertical seepage evolution law of the foundation treated by gravel pile.

Figure 7 illustrates the design idea of how this series of tests transforms the anti-liquefaction mechanism of gravel pile treatment site in engineering practice into model test scale for research.

From Model 1 to Model 2, the densification effect of gravel piles is actively designed, and the drainage and damping effects are avoided. It can be seen from Figure 7 that Model 1 is a typical liquefiable loose sand site, corresponding to the site state before treatment (void ratio $e = e_0$); Model 2 is a dense sand site with uniform density, which corresponds to the average density of soil around the pile after gravel pile treatment. We recognize that

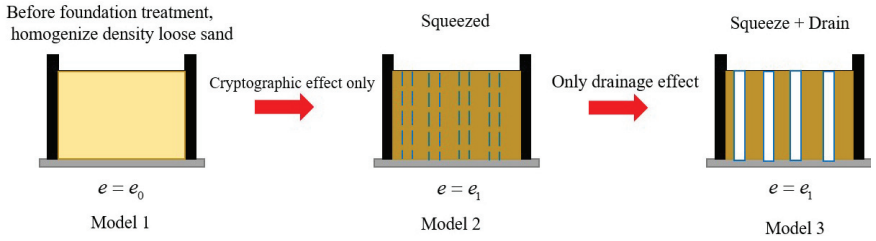

Figure 7 Conceptual diagram of three sets of model experimental design ideas.

the outspread compaction and vibration of the soil around the heap amid the development of the rock heap on the location will steadily diminish with the increment of the separate from the rock heap (as shown in Figure 7), which reflects the spatial variability of the density of the soil around the pile in the plane position, and the spatial variability of the stress state (static earth pressure coefficient K_o) and the permeability coefficient of the soil around the pile also exists. Within the Model 2 plan, the spatial inconstancy of the thickness of the soil around the heap is disentangled to the uniform thickness, and the spatial inconstancy of the stretch state and the penetrability coefficient of the soil isn't taken under consideration. There are two beginning focuses for this plan 1. At present, the gravel pile design in the specification only determines the target densified void ratio of the soil around the pile from the perspective of liquefaction discrimination, and does not consider the spatial variability of the density of the soil around the pile 2. At show, the physical recreation of tall gravity has not been able to recreate the method of gravel heap driving within the field by utilizing the mechanical arm beneath tall g esteem. Indeed with this capacity, the spatial changeability of soil thickness and stretch state around the heap caused by the driving handle is troublesome to be quantitatively assessed. Secondly, as shown in the dashed line of Model 2 in Figure 7, gravel piles should be arranged, but gravel material should be arranged should instead be piles with high density of surrounding soil material and material around the piles to avoid the drainage effect caused by high permeability coefficient of gravel material, while avoiding damping effect may be due to high modulus of gravel piles. With such a model test design, Model 1 and Model 2 can independently study the densification effect of gravel piles.

From Model 2 to Model 3, the drainage effect of gravel pile is actively designed, and the influence of damping effect on model response is avoided. The compactness of the soil around the pile in Model 3 ($e = e_1$) is consistent with that of the soil in Model 2. However, compared with Model 2, the dotted frame is arranged as the soil around the pile, and the corresponding position in Model 3 is arranged as coarse sand material to simulate the gravel pile material. Here, the following two points are mainly considered: first, the permeability coefficient of the pile material, and second, the stiffness of the pile material. For the first point, according to Seed&Booker's research proposal, the permeability coefficient of coarse sand material is two orders of magnitude larger than the permeability coefficient of soil around the pile, which meets the range of pile-soil permeability coefficient ratio in engineering practice, and some existing centrifugal model test designs also

basically adopt this design method. For the second point, in order to avoid introducing the damping effect in Model 3, the shear stiffness of the coarse sand will be greater than that of the real gravel material. If the coarse sand material is used, the damping effect will be inevitably introduced in Model 3. When the coarse sand material is used, the damping effect can be eliminated by designing a specific compactness to meet the pile-soil modulus ratio of the coarse sand and the soil around the pile is basically 1.0. In this way, Model 2 and Model 3 can study the drainage effect of gravel piles separately, and Model 3 is the coupling effect of gravel pile densification effect and drainage effect compared with Model 1.

Fujian sand + 10% silt (Qiantang River silt, 10% mass ratio) is selected as the foundation soil for this test, and Fujian sand with coarse grain size is selected as the gravel pile [30].

The relative density D of Model 1, =50% ($e_g = 0.705$), is a typical liquefiable medium dense sand site. According to the design method of anti-liquefaction treatment of gravel piles based on shear wave velocity proposed by Zhou Yanguo and others, the Model 2 dense sand model is designed to ensure the soil void ratio ($e_1 = 594$, Dr = 77%) when liquefaction does not occur under 0.1 g ($M_w = 7.5$) vibration. The layout parameters of gravel piles in Model 3 can be determined as follows according to Zhou Yanguo and other methods:

$$\frac{d}{s} = \frac{1}{\xi}\sqrt{\frac{4}{\pi}\frac{e_0 - e_1}{1 + e_1}} = \frac{1}{1.0}\sqrt{\frac{4}{\pi}\frac{0.705 - 0.594}{1 + 0.594}} = 0.3 \tag{53}$$

In the above formula, ξ is the correction factor of vertical settlement caused by gravel pile construction, with the range of 1.0–1.2. The ground settlement caused by the construction process is not considered in the model design stage, so $\xi = 1.0$; e_0 and e_1 are void ratio of foundation soil before and after gravel pile treatment. From this, the replacement rate $Ar = rd^2/(4s^2) = 7\%$ can be calculated.

Model 3 adds gravel piles on the basis of Model 2 dense foundation soil (soil between piles). The pile diameter d of gravel piles is 1.5 m according to Adalier et al. test. The pile spacing S is determined as 5.0 m. The centrifugal acceleration g value of this test is 50 g, so the diameter d and S of gravel pile corresponding to the model scale are 3 cm and 10 cm respectively [31].

In order to eliminate the possible shock absorption effect of gravel piles in Model 3, the compactness of Fujian coarse sand is specially designed. The damping effect can be reflected by the pile-soil stiffness ratio. The definition of Dashtietal is adopted here. The pile-soil modulus ratio is

defined as the ratio of the small strain shear modulus G_{ma} of the two materials. First, multi-stage loading isotropic consolidation wave velocity tests were performed on two saturated sand materials using a GDS dynamic triaxial instrument equipped with bending elements, and the following Hardin's equation was used to characterize the small-strain shear modulus of the materials:

$$G_{max} = AF(e)(\sigma_i' \cdot \sigma_j')^{n/2} \tag{54}$$

In the above formula, ρ Is saturated density; σ_i' and σ_j' is respectively effective principal stress in the plane where G_{max} is located; $\mathrm{F(e)} = 1/(0.3+0.7\mathrm{e}^2)$. The size of all unit specimens is 50 mm in diameter and 100 mm in height.

4.3.2 Verification of foundation seepage after gravel pile treatment

This section uses the results of the gravity model test to verify the expression of the radial and vertical seepage derived above. The permeability coefficient of foundation soil is $1.864\mathrm{e}^{-5}$ m/s (Dr = 77%), and the gravel pile material is $1.49\mathrm{e}^{-2}$m/s (Dr = 75%).

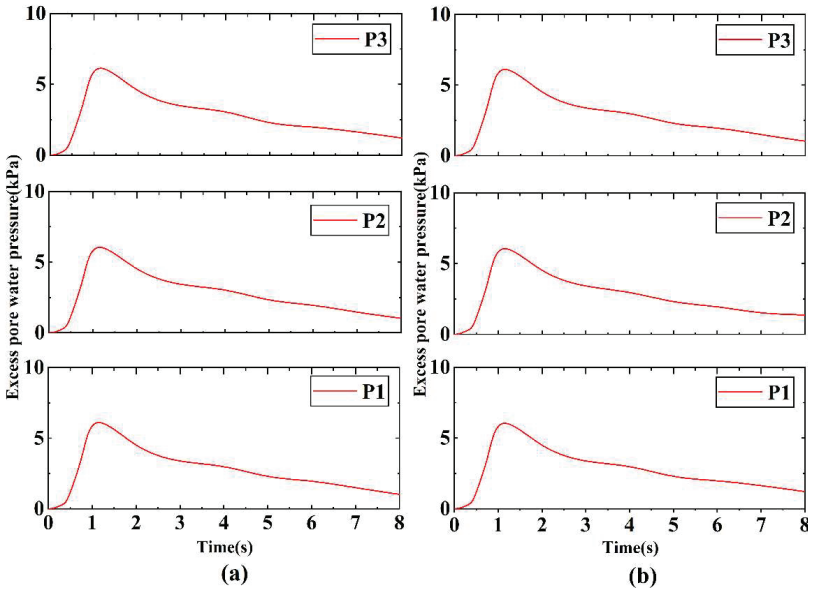

Figure 8 Superstatic hole compression time history in Model 3 (a) Vibration 1; (b) Vibration 1.

It should be noted that the formula derivation process in Section 3.3.2 assumes that the permeability coefficient of foundation soil is constant. However, Shahir et al. showed through theoretical analysis that the permeability coefficient of soil mass may increase 6–9 times during liquefaction, and Dashti et al. pointed out that the increase of the permeability coefficient of soil mass during liquefaction will further strengthen the seepage drainage during vibration, leading to the increase of final settlement. In order to avoid the change of the permeability coefficient of the foundation soil due to the ultra-high pore pressure caused by vibration, only vibration 1 and vibration 2 with the peak value of the table input ground motion less than 0.05 g are used in Model 3 [32, 33].

4.3.3 Verification of foundation densification after gravel pile treatment

Figure 9 appears the comparison comes about of time-history bends of overabundance inactive pore weight proportion between Demonstrate 1 and Demonstrate 2. It can be seen from the figure that after the soil is densified, the rate of abundance pore weight era amid all profound vibrations is essentially diminished, and this wonder is more self-evident within the

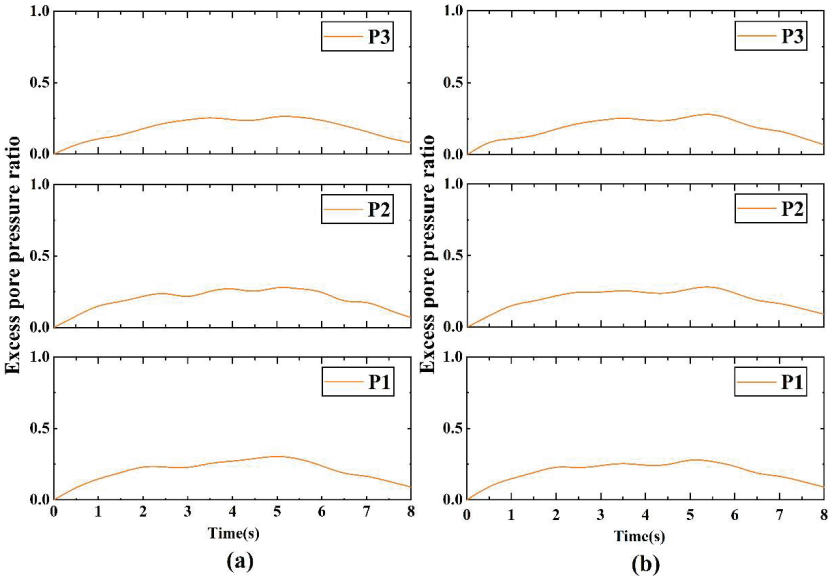

Figure 9 Comparison of Model 1 and Model 2 superstatic pore pressure ratios (a) Vibration 3; (b) Vibration 4.

profound reaction beneath little vibration. In vibration 3, the shallow layer (2.7 m) of Show 1 is melted (excess static pore pressure ratio $r_u = 1.0$), while Model 2 is not liquefied in the shallow layer. At other depths, the peak value of excess static pore pressure of Model 1 is significantly greater than that of Model 2. At the stage of dissipation and consolidation of pore pressure after earthquake, the dissipation rate of excess pore water pressure in Model 1 is significantly slower than that in Model 2, because loose sand produces greater settlement and higher excess pore pressure than dense sand under the same ground motion. It can moreover be seen from Figure 9 that the abundance pore weight proceeds to rise after the vibration stops within the center and shallow layers of the two bunches of models, which is caused by the moo penetrability coefficient of the establishment soil and the upward leakage of pore water driven by the angle of abundance pore weight from profound to shallow. The vibration start time is set to start at the 5th second. It can be seen from the figure that although the peak value of excess pore pressure at different depths of the two groups of models is different, the generation and dissipation of excess pore pressure are basically the same.

5 Conclusion

This paper presents an interpretive calculation strategy for the combined preparation of a block fabric pile considering the combined deformation of the pile. A single block fabric pile segment and the soil area around the pile within the impact range of a single pile are taken as the unit of study. The concept of normal excess pore water weight is proposed to consider the solidification deformation of the pile by rising the release of pore water during the solidification process to the reduction of the unit volume. The solidification conditions of the granular fabric pile composites are derived. The joint conditions are investigated in depth by using a dividing variable strategy through the suspicion of strain rise and the initiation of boundary conditions. The average superporous water pressure, average consolidation and overall consolidation of the composite foundation are obtained. For the input of seismic superposition, in this paper, based on the non-uniform seismic wave input strategy, the occurring seismic waves are converted into the same superposition acting on the artificially created viscoelastic boundary hubs by Matlab dialect program, and the same hub superposition is applied to the location soil finite component demonstration by the open source program OpenSees. The simulation process of earthquake incidence lays the foundation for carrying out the mechanical response of gravel pile structure

to deal with the foundation earthquake under the non-uniform incidence of seismic waves.

In this paper, the seismic response law of rock-pile structures was determined and analyzed using supergravity demonstration tests. The results show that: in the inclined shaft, the surface settlement is reduced by nearly 40–50% after the subsurface densification treatment, and the surface settlement is reduced by about 10–20% after the expanded waste effect, indicating that the subsurface densification treatment still plays a driving role in the settlement control in the inclined shaft; for the lateral displacement deformation, both the densification effect and the drainage effect can reduce the surface lateral displacement by more than 40%, and the contribution of both to the lateral displacement reduction The contribution of both to the reduction of lateral displacement is basically the same. The densification effect can significantly reduce the cumulative rate and peak level of excess pore pressure during vibration. The soil mass after densification has more noteworthy shear firmness and dilatancy, in this way decreasing the leftover distortion. The show test appears that the location settlement is diminished by approximately 45% after densification, so the densification impact plays a major part within the field settlement control.

References

[1] Zhao Minghua, Liu Dunping, Zhang Ling Analytical calculation of consolidation of composite foundation with bulk material piles considering pile consolidation deformation [J] Geotechnical Mechanics, 2010, 31 (2): 483–488.

[2] Taiheng W, Wei L, Meng C, et al. Analysis of Factors Influencing Mechanical Properties of Corrugated Steel Based on Entropy Method[J]. European Journal of Computational Mechanics, 2022: 539–554.

[3] Houalef I E, Bensaid I, Saimi A, et al. Free Vibration Analysis of Functionally Graded Carbon Nanotube-Reinforced Higher Order Refined Composite Beams Using Differential Quadrature Finite Element Method[J]. European Journal of Computational Mechanics, 2022: 505–538.

[4] Abdalla H M A. Pseudospectral approach to the shape optimization of beams under buckling constraints[J]. European Journal of Computational Mechanics, 2022: 351–386.

[5] Zhang Yuguo, Xie Kanghe, Ying Hongwei, etc Consolidation analysis of composite foundation of bulk material piles with double-sided

semi-permeable boundary [J] Journal of Geotechnical Engineering, 2005, 27 (3): 304–307.
[6] Xu Yang, Xie Kanghe, He Libo, etc Three-dimensional composite model and its application in the analysis of composite foundation with bulk piles [J] Journal of Rock Mechanics and Engineering, 2004, 23 (20): 3405–3412.
[7] Wang Ruichun, Xie Kanghe Analytical theory of consolidation of composite foundation with double-layer bulk material piles [J] Journal of Geotechnical Engineering, 2001, 23 (4): 418–422.
[8] Han J, Ye S L. Simplified method for consolidation rate of stone column reinforced foundations[J]. Journal of Geotechnical and Geoenvironmental Engineering, 2001, 127 (7): 597–603.
[9] Gray H. Simultaneous consolidation of contiguous layers of unlike compressible soils[J]. Trans., ASCE, 1945, 110: 1327–1344.
[10] Badanagki M, Dashti S, Kirkwood P. Influence of dense granular columns on the performance of level and gently sloping liquefiable sites[J]. Journal of Geotechnical and Geoenvironmental Engineering, 2018, 144 (9): 04018065.
[11] Bradley K, Mallick R, Andikagumi H, et al. Earthquake-triggered 2018 Palu Valley landslides enabled by wet rice cultivation[J]. Nature Geoscience, 2019, 12 (11): 935–939.
[12] Chen G, Wu Q, Zhou Z, et al. Undrained anisotropy and cyclic resistance of saturated silt subjected to various patterns of principal stress rotation[J]. Géotechnique, 2020, 70 (4): 317–331.
[13] Zhao M.H., Zhang L., Zou X.J., et al. Research progress of geocell-gravel pile bi-directional reinforced composite foundation[J]. Chinese Journal of Highways, 2009, 22 (1): 1–10.
[14] Li Chengcheng, Cao Zhenzhong, Li Ruishan Criterion and reliability analysis of site liquefaction sideshift grade [J] Journal of Geotechnical Engineering, 2016, 38 (9): 1668–1677.
[15] Lu Mengmeng, Xie Kanghe, Zhang Yuguo, etc Consolidation solution of composite foundation considering construction disturbance and load effect [J] Journal of Geotechnical Engineering, 2008, 30 (4): 549–554.
[16] Liang Tian Study on shear wave velocity characterization of liquefaction resistance of clayey sand [D] Hangzhou: Zhejiang University, 2013.
[17] Ma Weijia, Chen Guoxing, Qin You, etc Test on the influence of initial principal stress direction angle on liquefaction characteristics of saturated coral sand [J] Journal of Geotechnical Engineering, 2020, 42 (3): 592–600.

[18] Sun Haijun, Liu Songyu Theoretical analysis on the consolidation range of compacted silt by immersed gravel pile [J] Western Exploration Engineering, 2002, 14 (2): 39–41.
[19] Zhang Jianmin, Wang Gang Mechanism of large deformation of sand after liquefaction [J] Journal of Geotechnical Engineering, 2006, 28 (7): 835–840.
[20] Zhang Xudong, Zhang Yanmei, Liu Yingchun, etc Theoretical analysis of densification effect of gravel pile treating liquefiable foundation [J] Chinese Journal of Safety Science, 2005, 15 (6): 77–79.
[21] Zou Youxue, Wang Rui, Zhang Jianmin Seismic dynamic response analysis of gravel pile composite foundation in liquefiable site [J] Geotechnical Mechanics, 2019, 40 (6): 2443–2455.
[22] Zhang Yanmei, Zhang Hongru, Zhang Xudong Three-dimensional seismic response analysis of gravel pile composite foundation [J] Journal of Engineering Geology, 2008, 16 (1): 47–52.
[23] Tsutsui M. Behaviors of electromagnetic waves directly excited by earthquakes[J]. IEEE Geoscience and Remote Sensing Letters, 2014, 11 (11): 1961–1965.
[24] Shin J W, Oh S H, Yang W J. Review of Selection Technique of Design Seismic Wave According to Seismic Design Standards for Buildings[J]. Journal of the Architectural Institute of Korea, 2021, 37 (6): 199–206.
[25] Gao Zhi, Zhuo Weidong, Gu Yin Dynamic time-history analysis of subway station considering non-uniform seismic input [J] Earthquake Engineering and Engineering Vibration, 2016 (6): 56–63.
[26] Li Li, Jing Pengxu, Xu Qin Seismic response analysis of soil slope based on multi-point ground motion input [J] Journal of Disaster Prevention and Mitigation Engineering, 2018, 38 (2): 352–358.
[27] Kim Y S. Wave Passage Effect on the Seismic Response of a Building Considering Bedrock Shear Wave Velocity[J]. Journal of the Earthquake Engineering Society of Korea, 2014, 18 (2): 89–94.
[28] Han Junyan, Li Manjun, Zhong Zilan, etc Research on seismic response of soil layer based on shaking table test of buried pipeline under non-uniform excitation [J] Geotechnical Mechanics, 2020, 41 (5): 1653–1662.
[29] Zhao M, Gao Z, Wang P, et al. Response spectrum method for seismic analysis of monopile offshore wind turbine[J]. Soil Dynamics and Earthquake Engineering, 2020, 136: 106212.

[30] Yin Chao, Li Weihua, Zhao Chenggang Study on the amplification effect of slope terrain under oblique incidence of SV wave [J] Journal of Vibration Engineering, 2020, 33 (5): 971–984.
[31] Zhu Jun, Li Xiaojun, Liang Jianwen, etc The influence of tunnel # br # on the ground motion of the site under the three-dimensional oblique incidence of seismic wave [J] Journal of Civil Engineering, 2020, 53 (S1): 318–324.
[32] Xu L, Pan J, Leung C K Y, et al. Shaking table tests on precast reinforced concrete and engineered cementitious composite/reinforced concrete composite frames[J]. Advances in Structural Engineering, 2018, 21(6): 824–837.
[33] Zhao Minghua, He Junqiao, Cao Wengui, etc Research on vertical load transfer model and bearing capacity of foundation pile [J] Journal of Hunan University: Natural Science Edition, 2005, 32 (1): 37–42.
[34] Gu Y, Fu C C, Aggour M S. Topographic Effect on Seismic Response of a High-Pier Bridge Subjected to Oblique Incidence Waves[C]//Developments in International Bridge Engineering: Selected Papers from Istanbul Bridge Conference 2014. Springer International Publishing, 2016: 165–174.

Biography

Yin Zhenyu received the bachelor's degree in Hydrogeology and Engineering Geology from Jiaozuo Institute of Technology (now known as Henan Polytechnic University) in 2001, the master's degree in Geological Engineering from Henan Polytechnic University in 2008. He is currently working as a lecturer at the School of Civil and Transportation Engineering of Henan University of Urban Construction. His research areas and directions include pavement engineering and geotechnical engineering.